Physica C **191**, 485 (1992).
20. C. J. Muller *et al.*, *Phys. Rev. B* **53**, 1022 (1996), and references therein.
21. J. M. Tour *et al.*, *J. Am. Chem. Soc.* **117**, 9529 (1995).
22. C. Zhou, C. J. Muller, M. R. Deshpande, J. W. Sleight, M. A. Reed, *Appl. Phys. Lett.* **67**, 1160 (1995).
23. V. Mujica, M. Kemp, A. Roitberg, M. Ratner, *J. Chem. Phys.* **104**, 7296 (1996).
24. M. P. Samanta *et al.*, *Phys. Rev.* **53B**, R7626 (1996).
25. S. Datta *et al.*, *Phys. Rev. Lett.*, in press; W. Tian *et al.*, *Physica E*, in press.
26. We thank M. R. Deshpande for fruitful discussions and the Defense Advanced Research Projects Agency for support.

25 April 1997; accepted 22 August 1997

Depth Extent of the Lau Back-Arc Spreading Center and Its Relation to Subduction Processes

Dapeng Zhao,* Yingbiao Xu, Douglas A. Wiens, LeRoy Dorman, John Hildebrand, Spahr Webb

Seismic tomography and wave form inversion revealed that very slow velocity anomalies (5 to 7 percent) beneath the active Lau spreading center extend to 100-kilometer depth and are connected to moderately slow anomalies (2 to 4 percent) in the mantle wedge to 400-kilometer depth. These results indicate that geodynamic systems associated with back-arc spreading are related to deep processes, such as the convective circulation in the mantle wedge and deep dehydration reactions in the subducting slab. The slow regions associated with the Tonga arc and the Lau back arc are separated at shallow levels but merge at depths greater than 100 kilometers, suggesting that slab components of back-arc magmas occur through mixing at these depths.

Knowledge of the seismic structure beneath back-arc spreading centers is important because the width and depth of the slow-velocity regions below spreading centers provide constraints on the origin of back-arc spreading (*1*, *2*), the geochemical source of arc and back-arc magmas (*3*), the interaction between subduction and back-arc spreading (*1*), whether the mantle upwelling beneath spreading centers is passive or active, and to what depth the upwelling persists (*2*). A subduction zone with an associated back-arc spreading center and the existence of deep earthquakes immediately beneath the center provide an ideal geometry to image and understand back-arc spreading processes. The Tonga-Fiji region, which contains two-thirds of all deep earthquakes in the world, represents an optimal region for exploring these questions. Previous studies have discussed the seismic velocity anomalies due to the Tonga slab (*4*, *5*), but this work has been hampered by the poor distribution of seismic stations.

The installation (*6*) of 12 broadband stations in the Tonga and Fiji islands from November 1993 through December 1995 and a related 3-month deployment of 25 ocean bottom seismometers (OBS) (*7*) in the Lau back arc and the Tonga forearc provided a unique opportunity to determine high-resolution three-dimensional (3D) structure in this region (Fig. 1A). We used 41,471 arrival times from 926 earthquakes that occurred in the Tonga-Fiji region during the seismic experiment (Fig. 1B). Most of the events were associated with the subduction of the Tonga slab; they had a relatively uniform distribution in the entire upper mantle. This uniform distribution is an advantageous feature over other subduction zones, such as Japan and Alaska, where most of the seismicity is concentrated at depths shallower than 250 km (*8*, *9*). We picked about 8200 arrival times at the 12 land stations from the 926 earthquakes and about 2900 arrivals at the 25 OBS stations from 250 earthquakes that occurred during the OBS deployment. The picking accuracy is estimated to be 0.05 to 0.3 s. The remaining arrival times were recorded by stations reporting to the Preliminary Determination of Epicenters (PDE) with epicentral distances up to 90°. The PDE arrival times have lower quality (picking accuracy of 0.2 to 0.5 s), so they were assigned less than half the weight of the local data. All of the 926 earthquakes were recorded by more than 20 stations, and their hypocentral locations have a statistical accuracy of ±3 to 9 km. We also picked 450 arrival times at the 12 land and 25 OBS stations from 45 large (magnitude of 6.0 to 8.0) teleseismic events with epicentral distances from 30° to 90°, which were assigned the same weight as the local data in the inversion.

We used a tomography method (*9*) to determine the 3D *P* wave velocity structure in the Tonga-Fiji region (*9*, *10*) (Figs. 2 and 3). To confirm that the major velocity features were adequately resolved by the inversion, we conducted checkerboard resolution tests (*11*) (Fig. 4). The checkerboard test with a grid spacing of 50 km indicates good resolution for the area in and around the subducting Tonga slab and along the main line of OBSs (Fig. 4, A and B). For the test with a grid spacing of 70 km, the resolution is good for all the areas discussed (Fig. 4, C and D). We also conducted a number of inversions and resolution tests by changing the grid spacing, the grid configuration, and the initial model (*10*). The results show that the velocity structure in the study area (Fig. 3) can be resolved with a resolution of 50 to 70 km. This resolution scale is better than the 100- to 200-km resolution ob-

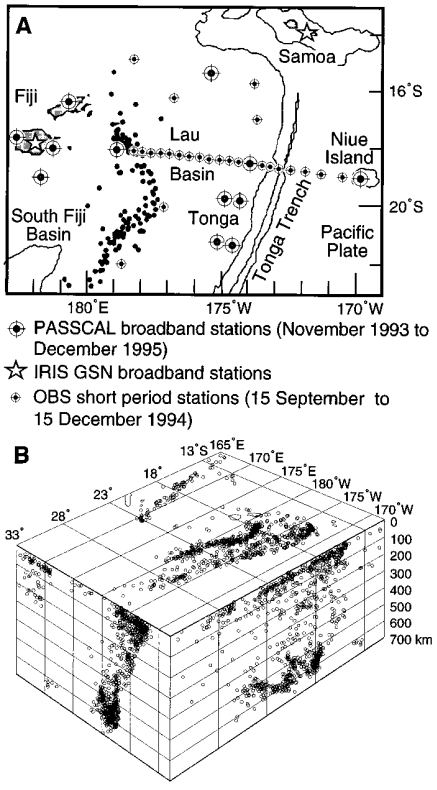

Fig. 1. (**A**) Map showing the seismometer deployments in the Fiji-Tonga region. Twelve broadband instrument island sites, 25 OBS sites, and two PDE sites (at Samoa and Fiji) recorded the data used in this study. A 2-year sample of deep earthquakes (depths of 300 to 680 km and $m_b > 4.8$) (dots) delineates the deep Tonga slab. PASSCAL, Program for Array Seismic Studies of the Continental Lithosphere; IRIS, Incorporated Research Institutions in Seismology; GSN, Global Seismographic Network. (**B**) Hypocentral distribution of the 926 earthquakes used in this study.

D. Zhao, Southern California Earthquake Center and Department of Earth Sciences, University of Southern California, Los Angeles, CA 90089, USA.
Y. Xu and D. A. Wiens, Department of Earth and Planetary Sciences, Washington University, St. Louis, MO 63130, USA.
L. Dorman, J. Hildebrand, S. Webb, Scripps Institution of Oceanography, University of California, San Diego, La Jolla, CA 92093, USA.

*To whom correspondence should be addressed. E-mail: dzhao@usc.edu

tained in previous studies (5).

The subducting Tonga slab was imaged as a 100-km-thick zone with a *P* wave velocity that is 4 to 6% higher than the surrounding mantle (Fig. 2). Beneath the Tonga arc and the Lau back arc, low-velocity anomalies of up to 7% are visible (Figs. 2 and 3). The slow-velocity anomaly beneath the Tonga arc represents a dipping region about 30 to 50 km above the slab, extending from the surface to about 140-km depth (Fig. 2). This feature is similar to the low-velocity features found beneath the Japan and Alaska volcanic fronts (8, 9). This slow anomaly probably represents the source zone for island arc magmas. Volatiles released from the subducting slab may reduce the melting point of the rock above and allow partial melting to produce arc magmas (3, *12*). Slow anomalies beneath areas of the active Central Lau Spreading Center (CLSC) and the Eastern Lau Spreading Center (ELSC) extend to depths of about 100 km. These depths correspond to regions where the primary magma genesis is expected to take place beneath an oceanic spreading center (*13*, *14*). The maximum heterogeneity of *P* wave velocity between the Lau back-arc basin and the Pacific Plate is about 13% at these depths. Slow anomalies are located to the west of the CLSC and ELSC (Figs. 2 and 3). Beneath 100-km depth, the amplitude of the back-arc anomalies is reduced, but a moderately slow anomaly (−2 to −4%) exists down to a depth of at least 400 km. To investigate the depth extent of slow anomalies in the Lau back arc with a different methodology, we inverted 16 wave forms from seven regional earthquakes recorded at the land stations to determine the 1D *S* wave structure beneath the Lau Basin (*15*). The inversion results (Fig. 5) show a similar level of velocity heterogeneity and depth distribution of the back-arc anomalies to that found in the *P* wave tomography. The level of *S* wave velocity heterogeneity reaches a maximum of about 18% between the Lau Basin and the old Pacific lithosphere at depths of 40 to 90 km (Fig. 5). The velocity difference decreases to about 2% at 180-km depth, but a small, poorly resolved difference persists to greater depths (*15*). There has been disagreement concerning the depth extent of slow-velocity anomalies at mid-ocean ridges (MORs) (*13*, *16*). Our results show that, at least for back-arc spreading centers, moderately slow velocity anomalies extend to depths of at least 400 km. These anomalies may reflect either the depth extent of oceanic spreading centers due to the depth of the associated upwelling patterns or processes endemic to back-arc spreading centers, perhaps due to interactions between the slab and the back arc.

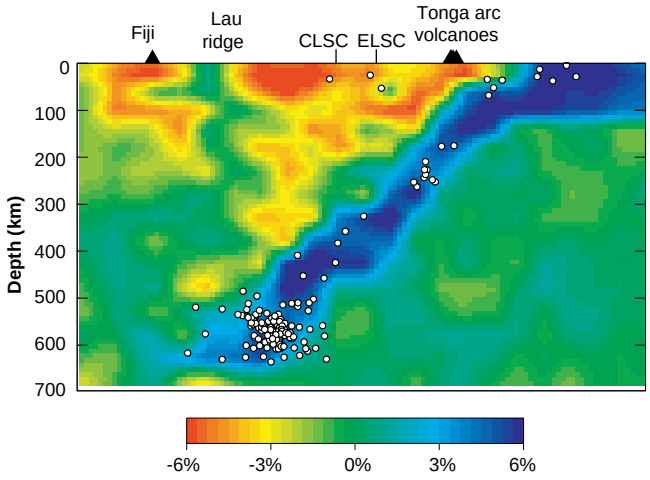

Fig. 2. East-west vertical cross section of a *P* wave velocity image from 0- to 700-km depth along the line AB (1220-km length) in Fig. 3A. Red and blue colors denote slow and fast velocities, respectively. Solid triangles denote active volcanoes. CLSC denotes the location of the Central Lau Spreading Center and ELSC denotes the location of the Eastern Lau Spreading Center. Earthquakes within a 40-km width from the cross section are shown as white circles. The velocity perturbation scale is shown at the bottom.

The slow-velocity anomalies at depths of 300 to 400 km (Fig. 2) could be caused by upwelling flow patterns in the back-arc region or by volatiles resulting from the deep dehydration reactions occurring in the subducting Tonga slab. Volatiles would have the effect of lowering the melting temperature and the seismic velocity and may produce small amounts of partial melt (*17*). Temperatures in fast subducting slabs like Tonga are low enough for water to reach the stability depths of dense hydrous magnesian silicate phases (*18*), which may allow water penetration down to depths of 660 km (*18*, *19*). The phase diagrams of important hydrous phases, the associated reaction kinetics, and the relevant mantle conditions (slab temperature and composition) are not known sufficiently well enough to predict the depth at which dehydration would occur. Partial melting of the back-arc region by volatiles from the deep slab may be important in localizing low seismic velocities in the back arc; the slow anomalies we observed at depths of 300 to 400 km may represent this process.

The slowest anomaly in the back-arc region is not found beneath the spreading center, but rather to the west. This is sim-

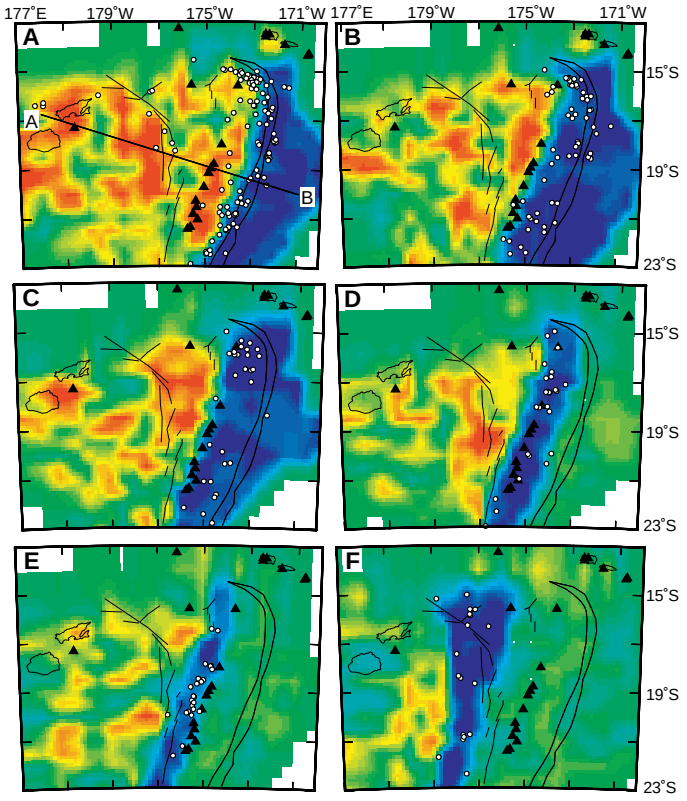

Fig. 3. *P* wave velocity images at (**A**) 25-, (**B**) 60-, (**C**) 100-, (**D**) 140-, (**E**) 230-, and (**F**) 430-km depths. Earthquakes within a 20-km depth range of the slice are shown as white circles. The long contour line to the right shows the Tonga trench. The lines in the middle show the back-arc spreading centers. The short contour lines to the left and in the upper right-hand corner show islands. Line AB in Fig. 3A shows the location of the cross section in Fig. 2. All other labeling is the same as in Fig. 2.

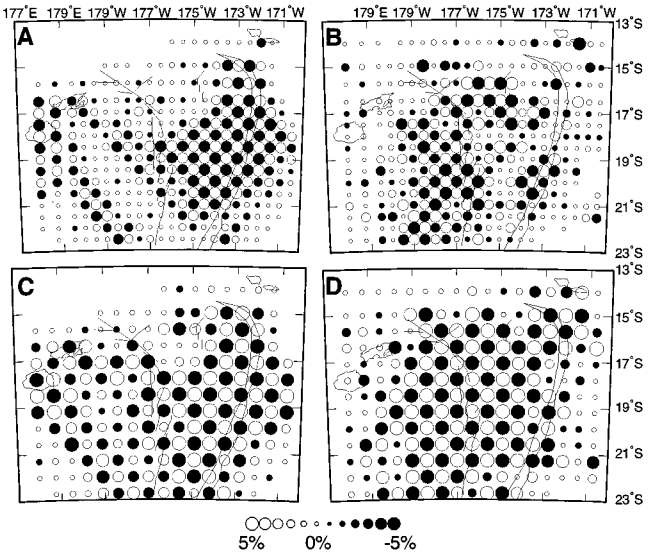

Fig. 4. Results of checkerboard resolution tests for *P* wave velocity structure at 25-km (**A** and **C**) and 480-km depths (**B** and **D**). The grid spacing is 50 km in (A) and (B) and 70 km in (C) and (D). Open and solid circles denote low and high velocities, respectively. The perturbation scales are shown at the bottom.

ilar to observations from several recent experiments along MORs, which showed smaller delay times for arrivals at stations near the MORs than for stations on the flanks (*20*, *21*). The faster arrivals near the ridge axis have been attributed to the alignment of anisotropic minerals in the mantle, with fast propagation for vertically traveling *P* waves caused by focused vertical flow beneath the spreading center. This effect may cause the arrivals at OBS stations near the spreading center to be faster than those off the ridge, causing the slowest anomalies to be displaced off the spreading center. The actual magma chamber beneath the spreading center would be expected to be less than 10 km in width (*22*), too small to image in this study.

Anisotropy may explain why the slowest velocities are not found immediately beneath the ridge, but it cannot explain why the western flank of the spreading center is slower than the eastern flank. This observation may be related to the ongoing tectonic processes in the Lau Basin. The CLSC, toward the west, is lengthening southward by rift propagation at the expense of the older ELSC, transferring the spreading activity westward (*23*). Our results suggest that this transfer may be favored by the proximity of the western ridge to upper mantle with the slowest velocities, which is also presumably the hottest mantle and the best source region for magma. Thus, the ridge propagation may be an attempt by the tectonic system to maintain the spreading center at or near the upper mantle magma source region.

The slow-velocity regions beneath the Tonga arc and the Lau back arc seem to be separated at shallow levels but merge at deeper levels (compare Fig. 3, A and C). This behavior suggests that although the arc and back-arc magma systems are separated at shallow levels, where most of the magma is generated, there may be some interchange between the magma systems at depths greater than 100 km. Interchange with slab-derived volatiles at depths greater than 100 km may help to explain some of the unique features in the petrology of back-arc magmas relative to typical MOR basalts, including excess volatiles and large ion lithophile enrichment (*24*).

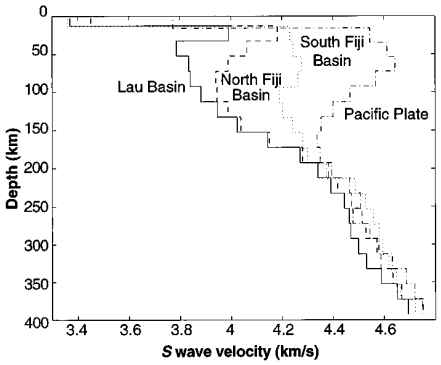

Fig. 5. *S* wave velocity models determined by inversions of entire regional vertical and radial wave forms recorded at island broadband seismic stations for various tectonic regions of the southwest Pacific.

REFERENCES AND NOTES

1. S. Uyeda, in *Island Arcs, Deep Sea Trenches and Back-Arc Basins*, M. Talwani and W. C. Pitman III, Eds. (American Geophysical Union, Washington, DC, 1977), pp. 1–14; M. N. Toksoz and P. Bird, in *Island Arcs, Deep Sea Trenches and Back-Arc Basins*, M. Talwani and W. C. Pitman III, Eds. (American Geophysical Union, Washington, DC, 1977), pp. 379–393; N. H. Sleep and M. N. Toksoz, *Nature* **33**, 548 (1971).
2. D. W. Forsyth, in *Mantle Flow and Melt Generation at Mid-Ocean Ridges*, J. Morgan, D. Blackman, J. Sinton, Eds. (American Geophysical Union, Washington, DC, 1993), pp. 1–65; D. L. Turcotte and J. P. Morgan, in *ibid.*, pp. 155–182.
3. S. M. Peacock, *Science* **248**, 329 (1990).
4. L. N. Huppert and C. Frohlich, *J. Geophys. Res.* **86**, 3771 (1981); G. Bock, *ibid.* **92**, 13863 (1987); K. M. Fischer, K. C. Creager, J. H. Jordan, *ibid.* **96**, 14403 (1991).
5. H. Zhou, *Phys. Earth Planet. Inter.* 61, **199** (1990); *J. Geophys. Res.* **101**, 27791 (1996); R. van der Hilst, *Nature* **374**, 154 (1995).
6. D. Wiens *et al.*, *IRIS Newsl.* **14**, 1 (1995).
7. R. Jacobson, L. Dorman, G. Purdy, A. Schultz, S. Solomon, *Eos* **72**, 506 (1991).
8. D. Zhao, D. Christensen, H. Pulpan, *J. Geophys. Res.* **100**, 6487 (1995).
9. D. Zhao, A. Hasegawa, S. Horiuchi, *ibid.*. **97**, 19909 (1992); D. Zhao, A. Hasegawa, H. Kanamori, *ibid.* **99**, 22313 (1994). A 3D net of nodes was set up in the Tonga-Fiji region with a horizontal grid spacing of 50 km and a vertical spacing of 25 to 50 km. Hypocentral locations of earthquakes and velocities at the grid nodes were taken as unknown parameters. The velocity at any point was calculated by linearly interpolating the velocities at the eight grid nodes surrounding that point. An efficient 3D ray tracing technique was used to calculate ray paths and travel times. A conjugate gradient algorithm [C. Paige and M. Saunders, *ACM Trans. Math. Software* **8**, 43 (1982)] was used to solve the large sparse system of observational equations by regularizing the solution in a damped least-squares fashion [K. Aki and W. Lee, *J. Geophys. Res.* **81**, 4381 (1976)]. The nonlinear tomographic problem was solved by iteratively conducting linear inversions. Hypocenters were relocated in the inversion process. For the local data from the 926 events (Fig. 1), raw arrival times were used in the inversion. For the teleseismic data with epicentral distances greater than 30°, we used the relative travel time residuals by removing the average of the travel time residuals for each station, to remove the effect of the structures outside the study area.
10. D. Zhao *et al.*, *Eos (Fall Suppl.)* **77**, 498 (1996). The starting 1D model for the inversion was the IASP91 Earth model (*25*), but the crustal thickness has lateral variations according to a seismic refraction survey along the line of OBS stations (*26*) and the inversion of land station wave forms (*15*). The crustal thickness varies from 5 to 24 km, with the thickest crust beneath the Lau Ridge, Tonga arc, and Fiji Islands. Numerous previous studies (*4*, *5*) have demonstrated the existence of the Tonga slab, which is at least 100 km thick with a *P* wave velocity of up to 7% faster. The slab substantially perturbs ray trajectories, such that the ray path perturbation can be over 100 km from that in the 1D Earth model (*4*, *9*). Our primary concern in this study is the precise structure below the Lau Basin and in the mantle wedge. For this purpose, it was necessary to use a starting model incorporating the a priori slab information (*8*, *9*) because we hoped to resolve the anomalies in the Lau Basin with a resolution of 50 to 70 km. We introduced the Tonga slab into the model using the slab geometry determined by Billington (*27*). The introduction of the slab into the model reduced the nonlinearity of the problem because seismic rays are traced realistically from the beginning of the inversion (*8*, *9*). We conducted a number of inversions by changing the initial slab thickness from 50 to 150 km and the initial slab velocity from 1 to 9% faster than the normal mantle. We also conducted inversions without the slab in the starting model. All of the inversions imaged the very slow velocity anomalies beneath the Lau spreading center to about 100-km depth and the moderately slow anomalies to about 400-km depth, but there are 1 to 2.5% changes in the amplitudes of the anomalies and up to 10% changes in the final travel time residuals. The inversion with the starting model that included a 100-km-thick slab and that was 6% faster than the normal mantle resulted in the best fit of model to data. The results of this inversion are shown in Figs. 2 and 3.
11. To make a checkerboard in the resolution tests, we assigned positive and negative velocity anomalies

with magnitudes of 5% to the 3D grid nodes. Synthetic data were calculated for the checkerboard model. Then we added random errors to the synthetic data and inverted them with the same algorithm that we used for the observed data. The inverted image of the checkerboard suggests where the resolution is good and where it is poor. The checkerboard resolution tests and other synthetic tests we conducted showed that both the high-velocity Tonga slab and the low-velocity back arc and mantle wedge were reliably resolved and that there was no trade-off between them.

12. Y. Tatsumi, *J. Geophys. Res.* **94**, 4697 (1989); J. H. Davies and D. J. Stevenson, *ibid.* **97**, 2037 (1992).
13. Y. Zhang and T. Tanimoto, *Nature* **355**, 45 (1992); T. Tanimoto and D. J. Stevenson, *J. Geophys. Res.* **99**, 4549 (1994).
14. Y. Shen and D. W. Forsyth, *J. Geophys. Res.* **100**, 2211 (1995).
15. Y. Xu and D. Wiens, *ibid.*, in press. To invert regional wave forms we used a nonlinear inversion method that adopts a reflectivity formalism (*28*) to compute the partial derivatives. This method allows the entire regional distance (400- to 1500-km range) wave form to be inverted from *P* wave arrival to surface waves at frequencies between 0.01 and 0.055 Hz. Broadband seismograms from earthquakes of 10 to 240 km deep that propagate almost entirely within one of the tectonic regions of the southwest Pacific were used in the wave form inversion. Parameter variances and resolution tests suggest that the results are well constrained to depths of about 200 km. The *S* wave velocities from the wave form inversion and the *P* wave velocities from the tomography would not necessarily show the same structure. The larger total heterogeneity from the wave form inversion may result from a greater effect of partial melt beneath the Lau back arc on *S* wave velocity than on *P* wave velocity (*9*, *29*).
16. W. Su, R. L. Woodward, A. M. Dziewonski, *Nature* **360**, 149 (1992).
17. G. Nolet and A. Zielhuis, *J. Geophys. Res.* **99**, 15813 (1994); G. Nolet, in *Processes of Deep Earth and Planetary Volatiles*, K. Farley, Ed. (American Institute of Physics, New York, 1995), pp. 22–32.
18. A. B. Thompson, *Nature* **358**, 295 (1992); H. Staudigel and S. D. King, *Earth Planet. Sci. Lett.* **109**, 517 (1992).
19. A. Navrotsky and K. Bose, in *Processes of Deep Earth and Planetary Volatiles*, K. Farley, Ed. (American Institute of Physics, New York, 1995), pp. 221–228.
20. D. Toomey *et al.*, *Eos (Fall Suppl.)* **77**, 652 (1996).
21. D. Blackman *et al.*, *Geophys. J. Int.* **127**, 415 (1996).
22. J. S. Collier and M. C. Sinha, *J. Geophys. Res.* **97**, 14031 (1992).
23. L. M. Parson and I. C. Wright, *Tectonophysics* **263**, 1 (1996); B. Taylor, K. Zellmer, F. Martinez, A. Goodliffe, *Earth Planet. Sci. Lett.* **144**, 35 (1996).
24. J. A. Pearce *et al.*, in *Volcanism Associated with Extension at Consuming Plate Margins*, J. L. Smellie, Ed. (Geological Society, London, 1992), pp. 53–75; J. W. Hawkins, in *Active Margins and Marginal Basins of the Western Pacific*, B. Taylor and J. Natland, Eds. (American Geophysical Union, Washington, DC, 1995), pp. 125–173.
25. B. L. N. Kennett and E. R. Engdahl, *Geophys. J. Int.* **105**, 429 (1991).
26. W. Crawford, S. Webb, J. Hildebrand, *Eos (Fall Suppl.)* **77**, 478 (1996).
27. S. Billington, thesis, Cornell University, Ithaca, NY, (1980).
28. B. L. N. Kennett, *Seismic Wave Propagation in Stratified Media* (Cambridge Univ. Press, Cambridge, 1983); G. E. Randall, *Geophys. J. Int.* **118**, 245 (1994).
29. U. H. Faul, D. R. Toomey, H. S. Waff, *Geophys. Res. Lett.* **21**, 29 (1994).
30. We thank M. Bevis, W. Crawford, K. Draunidalo, S. Escher, T. Fatai, H. Gilbert, S. Helu, K. Koper, M. McDonald, J. McGuire, B. Park-Li, G. Prasad, E. Roth, A. Sauter, P. Shore, and L. Vuetibau for their assistance during the seismic experiment and at the data-processing stage and G. Abers and an anonymous referee for thoughtful reviews, which improved the manuscript. Broadband seismographs were obtained from the PASSCAL program of the Incorporated Research Institutions in Seismology (IRIS). Supported by the NSF under grants EAR-9219675, OCE-9314446, and EAR-9614502. This paper is Southern California Earthquake Center publication 386.

8 May 1997; accepted 18 August 1997

Microscopic Molecular Diffusion Enhanced by Adsorbate Interactions

B. G. Briner,* M. Doering, H.-P. Rust, A. M. Bradshaw

The diffusion of carbon monoxide molecules on the (110) surface of copper was investigated in the temperature range between 42 and 53 kelvin. The activation energy for thermal motion was determined directly by imaging individual molecular displacements with a scanning tunneling microscope. An attractive interaction between carbon monoxide molecules gave rise to the formation of dimers and longer chains. Carbon monoxide chains diffused substantially faster than isolated molecules although the chains moved by a sequence of single-molecule jumps. A higher preexponential factor in the Arrhenius law was found to be responsible for the observed efficiency of chain hopping.

Adsorbate diffusion is of fundamental importance for surface chemistry (*1*). It is often the rate-limiting step in catalysis because adsorbed atoms or molecules first have to reach a reaction partner or an active site (*2*) on the surface before a reaction can take place. Efforts to study diffusion on a microscopic scale are needed to understand how interactions with the surface and with neighboring adsorbates influence the way a particle diffuses. This information forms an indispensable basis to model diffusion on a macroscopic scale under the conditions that prevail in catalysis. This report focuses on the microscopic diffusion of CO molecules on Cu(110). Carbon monoxide is only weakly chemisorbed on Cu(110) (*3*), and helium scattering experiments have suggested very low diffusion barriers (*4*). Therefore, CO can serve as a test case to assess whether diffusion of the often weakly bound molecules that are of interest in surface chemistry is accessible to microscopic observation.

All experiments were performed with an Eigler-type, variable temperature scanning tunneling microscope (STM), which operates in an ultrahigh vacuum and can be cooled down to 4 K (*5*). We applied experimental techniques similar to those used in earlier STM-based studies on diffusion (*6*), but the present results differ in two ways from earlier findings. First, we observed that the activation energy for CO diffusion was substantially lower than the barrier heights that had been determined before with microscopic imaging techniques. This result indicates that the STM can indeed be used to probe the motion of weakly bound species and that the artifacts of STM-induced adsorbate motion that were reported in (*7*) can be avoided. Second, our study went beyond the observation of single-particle diffusion. It was found that CO forms chains on Cu(110). These chains experienced considerable thermal mobility in the same temperature range in which the diffusion of isolated molecules was observed. By comparing the diffusion of single molecules with that of CO chains, we could investigate the influence of molecular interactions on the adsorbate mobility. Cluster diffusion was first investigated by field ion microscopy (FIM) (*8*). Although this technique is limited to the study of strongly bound transition metal adatoms, it could provide detailed information on the characteristics of cluster diffusion. In general, the rule that cluster mobility decreases strongly with increasing cluster size was confirmed, but FIM experiments have also demonstrated that there are exceptions to this rule. Iridium tetramers have been found to diffuse faster than trimers (*9*), and for rhenium on tungsten(211), dimers have been shown to be faster than single adatoms (*10*). The reason for this enhanced mobility is a reduction of the activation energy; adding an atom to a cluster can strengthen the cluster bonds at the expense of weakening the bonds to the substrate (*11*–*13*). We observed that CO chains also experienced an enhanced mobility, but in contrast to the metal clusters described above, no reduced activation energy for chain diffusion was found.

Samples were prepared by adsorbing CO onto the clean Cu(110) substrate at a temperature of about 60 K. We found that under these adsorption conditions, CO still has substantial mobility. This mobility is inferred

Fritz-Haber-Institut der Max-Planck-Gesellschaft, Faradayweg 4-6, 14195 Berlin, Germany.

*To whom correspondence should be addressed. E-mail: briner@fhi-berlin.mpg.de